HHS Public Access

Author manuscript

J Neurochem. Author manuscript; available in PMC 2020 January 03.

Published in final edited form as:

J Neurochem. 2019 January ; 148(2): 219–237. doi:10.1111/jnc.14634.

Diet-Induced Insulin Resistance Elevates Hippocampal Glutamate as well as VGLUT1 and GFAP Expression in AβPP/PS1 Mice

Erin R. Hascup[1,2], **Sarah O. Broderick**[1], **Mary K. Russell**[3], **Yimin Fang**[4], **Andrzej Bartke**[4], **Heather A. Boger**[3], and **Kevin N. Hascup**[1,*]

[1]Department of Neurology, Center for Alzheimer's Disease and Related Disorders, Neurosciences Institute, Southern Illinois University School of Medicine, Springfield, IL, USA

[2]Department of Pharmacology, Southern Illinois University School of Medicine, Springfield, IL, USA

[3]Department of Neuroscience, Center on Aging, Medical University of South Carolina, Charleston, SC, USA

[4]Division of Geriatric Research, Department of Internal Medicine, Southern Illinois University School of Medicine, Springfield, IL, USA

Abstract

The symptomologies of Alzheimer's disease (AD) develop over decades suggesting modifiable life-style factors may contribute to disease pathogenesis. In humans, hyperinsulinemia associated with type 2 diabetes mellitus increases the risk for developing AD and both diseases share similar age-related etiologies including amyloidogenesis. Since we have demonstrated that soluble $A\beta_{42}$ elicits glutamate release, we wanted to understand how diet-induced insulin resistance alters hippocampal glutamate dynamics, which are important for memory formation and consolidation. Eight to twelve week-old C57BL/6J and AβPP/PS1 mice were placed on either a low-fat diet (LFD) or high-fat diet (HFD) for eight months. A HFD led to significant weight increases as well as impaired insulin sensitivity, glucose tolerance, and learning in both C57BL/6J and AβPP/PS1 mice. AβPP/PS1 LFD mice had elevated hippocampal basal as well as stimulus-evoked glutamate release that was further increased with consumption of a HFD. Immunohistochemistry indicated

*Corresponding author: Hascup, KH, Department of Neurology, Center for Alzheimer's Disease and Related Disorders, Neurosciences Institute, Southern Illinois University School of Medicine, P.O. Box 19628, Springfield, IL 62794-9628, USA, Tel: 217-545-6994; khascup49@siumed.edu.

Author Contributions

KNH conceived the study, conducted the experiments, analyzed the data, and wrote the manuscript. SOB assisted with experiments and data analysis. MKR performed the IHC and corresponding data analysis. HAB supervised IHC and revised the manuscript. YF and AB performed the ELISA, assisted with data analysis, and revised the manuscript. ERH conceived and supervised the study and revised the manuscript. All authors approved the final version of the manuscript.

Conflicts of Interest

The authors declare no competing financial interests.

Open Science Badges

This article has received a badge for *__Open Materials__* and for *__Open Data__* because it made the data publicly available. The data can be accessed at DOI: 10.13140/RG.2.2.11180.10888 and https://osf.io/5whvu (figures for data) and https://osf.io/gd5vf (materials and methods) . The complete Open Science Disclosure form for this article can be found at the end of the article. More information about the Open Practices badges can be found at https://cos.io/our-services/open-science-badges/.

an increase in vesicular glutamate transporter 1 and glial fibrillary acidic protein density in hippocampal subregions corresponding with this elevated extracellular glutamate. While no differences in hippocampal plaque load were observed, the elevated astrogliotic response surrounding the plaques in AβPP/PS1 HFD mice may have been a compensatory mechanism to control plaque accumulation. These data support that AβPP/PS1 mice have chronically elevated extracellular glutamate that is exacerbated by a HFD and that modifiable life-style factors such as obesity-induced insulin resistance can contribute to AD pathogenesis.

Graphical Abstract

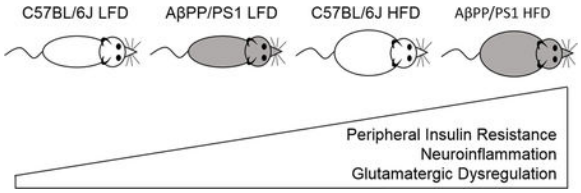

The aim of the present study was to address how obesity-induced insulin resistance alters hippocampal glutamate dynamics in both cognitively normal and AβPP/PS1 mice predisposed to Alzheimer's disease (AD) pathology. AβPP/PS1 mice presented with insulin resistance, neuroinflammation, and elevated hippocampal glutamate dynamics compared to C57BL/6J mice. A high-fat diet exacerbated all of these phenotypes in C57BL/6J and AβPP/PS1 mice. The current study highlights elevated hippocampal glutamatergic neurotransmission associated with a diabetic phenotype. Additionally, our laboratory has observed a consistent theme of elevated hippocampal glutamate across ages of AβPP/PS1 mice, which may serve as an early therapeutic biomarker for AD pathogenesis.

Keywords

Diabetes; Amyloid-beta; Cognition; Alzheimer's disease; Astrogliosis; Excitotoxicity

Introduction

Alzheimer's disease (AD) is an age-related neurodegenerative disorder characterized by a slow, but progressive, accumulation of extracellular aggregated beta-amyloid (Aβ) and intracellular hyperphosphorylated tau tangles (Jack *et al.* 2013). This accumulation leads to alterations in neurotransmitter dynamics, synapse loss, and cerebral atrophy that culminates in the eventual cognitive and functional decline associated with the disorder (Mota *et al.* 2014). To date, current therapeutics target cholinesterase inhibitors, to increase acetylcholine levels, or antagonism of the N-methyl-D-aspartate (NMDA) receptor, to prevent glutamate mediated excitotoxicity (Cummings *et al.* 2014; Godyń *et al.* 2016). However, these therapies have limited efficacy, only treat symptoms, and do not decelerate disease progression, possibly because they are administered at advanced AD stages. Without a well-established biomarker for AD, early diagnosis is difficult and underscores the lack of disease-modifying pharmacotherapy options. To further complicate diagnosis, evidence supports that AD symptomology develops over decades and modifiable lifestyle factors,

such as obesity-induced type 2 diabetes mellitus (T2DM), may contribute to AD progression (Barnes and Yaffe 2011).

The peptide hormone, insulin, regulates glucose uptake and storage in the periphery and brain for use in energy production (De Felice 2013). However, excessive caloric consumption, particularly of hydrogenated or saturated fats, promotes a cascade of metabolic events starting with elevated circulating insulin concentrations that leads to insulin resistance and increases the risk factor for developing T2DM (Holland *et al.* 2007). In fact, T2DM and AD share several age-related etiologies including hyperinsulinemia, insulin resistance, hyperglycemia, amyloidogenesis and memory impairment (Zhao and Townsend 2009; Talbot *et al.* 2012; Moloney *et al.* 2010). These similar symptomologies suggest insulin resistance and the subsequent onset of T2DM is a risk for developing AD (Vandal *et al.* 2014). In support of this, the Mayo Clinic Alzheimer Disease Patient Registry has reported that 80% of their AD patients had either T2DM or impaired glucose tolerance (Janson *et al.* 2004) and T2DM in midlife increases the odds for developing mild cognitive impairment or AD later in life by 1.5- to 2-fold (Allen *et al.* 2004; Ott *et al.* 1999; Arvanitakis *et al.* 2004). While the mechanistic link between T2DM and AD is not fully elucidated, the metabolic hypothesis of AD supports altered insulin signaling promotes a cascade of neurological events that initiate the pathogenesis of AD (Hoyer 2002). For example, brain insulin degrading enzyme (IDE) regulates the metabolism of both insulin and Aβ, but at a lower affinity for the latter. As such, hyperinsulinemia prevents IDE from degradation of monomeric Aβ leading to its accumulation and aggregation (Farris *et al.* 2003). These small molecular weight isoforms of Aβ (monomers, dimers, and trimers) are hypothesized to be the bioactive component that causes synaptic dysfunction, neurotoxicity, and the eventual neurodegeneration associated with AD (Jin and Selkoe 2015; Yang *et al.* 2017).

Prior studies have demonstrated that soluble $A\beta_{42}$ elicits glutamate release through the α7 nicotinic acetylcholine receptor (α7nAChR; Talantova et al., 2013; Hascup and Hascup, 2016). Because of glutamate's role in learning and memory, it is hypothesized that persistent, excessive synaptic glutamate overstimulates the NMDA receptor thereby preventing detection of physiological signals leading to cognitive impairment (Parsons *et al.* 2007). In fact, our laboratory has demonstrated that double transgenic mice expressing a mutant amyloid precursor protein (Mo/HuAPP695swe) and Presenilin 1 (PS1-dE9) genes (AβPP/PS1) have elevated hippocampal glutamate as early as 2–4 months of age; prior to the onset of cognitive decline (Hascup and Hascup 2015). While previous studies have demonstrated that HFD exacerbates cognitive decline and disease neuropathology in animal models of AD (Vandal *et al.* 2014; Knight *et al.* 2014; Thériault *et al.* 2016; Julien *et al.* 2010), alterations to memory associated neurotransmitters have not been elucidated. The aim of the present study was to address how obesity-induced insulin resistance alters glutamate dynamics in both cognitively normal and AβPP/PS1 mice predisposed to AD pathology. Since previous studies have shown that HFD affects memory in cognitively normal rodents (Kanoski and Davidson 2011; Cordner and Tamashiro 2015), non-AD control mice help to understand changes associated with, or independent from, the metabolic hypothesis of AD pathogenesis.

Materials & Methods

Animals:

Protocols for animal use were approved by the *Laboratory Animal Care and Use Committee* at Southern Illinois University School of Medicine (Protocol #219–14-003) and the study was not preregistered. Eight to twelve week old male, C57BL/6J (RRID:IMSR_JAX: 000664) and AβPP/PS1 (RRID:MMRRC_034832-JAX; Mo/HuAPP695swe / PS1-dE9), mice were obtained from Jackson Laboratory (Bar Harbor, ME), and group housed on a 12:12 hour light: dark cycle with food and water available *ad libitum*. All experiments were conducted during the light phase. Genotype was confirmed by TransnetYX®, Inc (Cordova, TN). All mice were ear tagged with unique numerical identifiers so as to blind researchers throughout the experimental paradigms. Pseudo randomization using the Microsoft Excel 2013 randomization function to generate random decimal numbers between 0 and 1 for each mouse and dietary treatment. These random numbers were then sorted into ascending order generating a list that categorized mice into the following groups C57BL/6J low fat diet (LFD), C57BL/6J HFD, AβPP/PS1 LFD, and AβPP/PS1 HFD. Similar methodology was used to determine the order of which animals were assessed. A n=15 for all treatment groups was allocated at study initiation; however, due to animal loss from normal aging and disease progression, the following indicates the remaining number of animals available at the end of the 8 month dietary treatment: C57BL/6J LFD (n=14), C57BL/6J HFD (n=11), AβPP/PS1 LFD (n=11), AβPP/PS1 HFD (n=12). All of these remaining mice underwent blood glucose monitoring, cognitive assessment, *in vivo* glutamate recordings, and immunohistochemical (IHC) analysis except for one AβPP/PS1 HFD mouse that died during *in vivo* glutamate recordings as outlined in Figure 1A. Following *in vivo* electrochemistry, all mice were euthanized by an overdose of isoflurane followed by rapid decapitation with sharp scissors.

Chemicals:

All chemicals were prepared and stored according to manufacturer recommendations unless otherwise noted. L-glutamate oxidase (EC 1.4.3.11) was obtained from Cosmo Bio USA Co. (Carlsbad, CA; Cat: YMS-80049) and reconstituted in distilled, deionized water to make a 1U/μl stock solution and stored at 4°C. Sodium phosphate monobasic monohydrate (Cat: BP330–500), sodium phosphate dibasic anhydrous (Cat: S375–500), 1,3-phenylenediamine dihydrochloride (mPD; Cat: P017225G), sodium chloride (Cat: S271–3), calcium chloride dehydrate (Cat: BP510–100), dextrose monohydrate (Cat: D15–500), and hydrogen peroxide (H_2O_2; Cat: H325–100) were obtained from Thermo Fisher Scientific (Waltham, MA). L-glutamic acid sodium salt (Cat: G1626), potassium chloride (Cat: P9333), bovine serum albumin (BSA; Cat: A3059), glutaraldehyde (Cat: G5882), dopamine hydrochloride (DA; Cat: H8502), L-ascorbic acid (AA; Cat: A7056), and dibutyl phthalate and xylene (DPX; Cat: 06522) were obtained from Sigma-Aldrich Co. (St. Louis, MO). Rabbit polyclonal glial fibrillary acidic protein (GFAP) antibody was obtained from Dako (Carpinteria, CA; RRID:AB_10013382). Guinea pig polyclonal vesicular glutamate transporter 1 (VGLUT1) antibody was obtained from Millipore (Burlington, MA; RRID:AB_2301751). Biotinylated goat anti-rabbit serum (RRID:AB_2313606), biotinylated goat anti-guinea pig serum (RRID:AB_2336132), avidin-biotin complex (ABC) kit (RRID:AB_236818), and VIP peroxidase substrate kit (RRID:AB_2336819) were obtained from Vector Laboratories

(Burlingame, CA). Amylo-Glo® RTD™ with ethidium bromide (EtBr) was obtained from Biosensis (Temecula, CA; Cat: TR-400-AG).

Low-fat and high-fat diet:

All mice were switched from standard rodent chow (13% kcal fat, 57% kcal carbohydrate, 30% kcal protein, 4% sucrose, 4.09 kcal/gm; LabDiet, St. Louis, MO; Cat: 5001) to either a LFD (10% kcal fat, 70% kcal carbohydrate, 20% kcal protein, 7% sucrose, 3.85 kcal/gm; Cat: D12450J) or HFD (60% kcal fat, 20% kcal carbohydrate, 20% kcal protein, 7% sucrose, 5.24 kcal/gm; Cat: D12492) obtained from Research Diets Inc. (New Brunswick, NJ). A LFD diet was used as the control diet so as to match protein and sucrose content with the HFD. Mouse weight was monitored throughout the study (Fig 1B).

Intraperitoneal (ip) Insulin tolerance test (ITT) and Glucose Tolerance Test (GTT):

To determine insulin sensitivity, an initial blood glucose measurement (time = 0) was taken from the tail vein of four hour fasted mice and measured using a Presto® glucometer (AgaMatrix, Salem, NH) followed by ip injection of 1 IU / kg body weight (b.w.) Humulin® R (Henry Schein, Melville, NY: Cat: 1238578). To determine glucose tolerance, an initial blood glucose measurement was taken (time = 0) from fifteen hour fasted mice followed by an ip injection of 2 g of glucose / kg b.w. Following either injection, blood glucose levels were measured sequentially at 15, 30, 45, 60, and 120 min (Fang *et al.* 2017).

Morris water maze:

The MWM paradigm consisted of 2 consecutive training days where the mouse learned to remain on the platform for 60 seconds before rescue. For the first training day, a visible platform protruded 1 cm out of the opaque pool of water to aid in platform location. Mice underwent three consecutive 60 second maximum trials with a 15 minute inter-trial interval. On the second training day, the visible platform was removed and mice underwent 3 training blocks (30 minute inter-block interval) of 3, sixty second maximum trials (15 minute inter-trial interval) to learn the location of the submerged platform (1 cm below the surface). Starting quadrant was varied for each trial. The probe challenge consisted of a single 60 s trial. The ANY-maze video tracking system (Stoelting Co., Wood Dale, IL; RRID:SCR_014289) records and analyzes maze navigation. The three training sessions for Day 1 and for each training block in Day 2 were averaged.

Enzyme-based microelectrode arrays:

Enzyme-based MEAs with platinum (Pt) recording surfaces were fabricated, assembled, coated, and calibrated for *in vivo* mouse glutamate measurements as previously described (Burmeister et al., 2000; Hascup et al., 2006; Hascup et al., 2013). One of the MEA (Quanteon LLC; Cat: R2) Pt sites was coated with an L-glutamate oxidase, BSA, glutaraldehyde solution. BSA and glutaraldehyde increase the adhesion and crosslink L-glutamate oxidase to the MEA surface, while L-glutamate oxidase enzymatically degrades glutamate to α-ketoglutarate and H_2O_2, the electroactive reporter molecule. The second Pt recording site (self-referencing or sentinel site) was coated with a BSA and glutaraldehyde solution that is unable to enzymatically generate H_2O_2 from L-glutamate. A potential of

+0.7V vs a Ag/AgCl reference electrode was applied to the Pt recording surfaces, resulting in a two electron oxidation of H_2O_2 and the subsequent current was amplified and digitized by the Fast Analytical Sensing Technology (FAST) 16mkIII (Quanteon, LLC; Nicholasville, KY) electrochemistry instrument.

mPD Electropolymerization:

Pt recording surfaces were electroplated with 5 mM mPD in 0.05 M phosphate buffered saline (PBS) for 20 min to restrict the passage of AA, DA, uric acid, and 3,4-dihydroxyphenylacetic acid (Hascup *et al.* 2016).

Calibration:

MEAs were calibrated in 0.05 M PBS (37°C) to create a standard curve for the conversion of current to glutamate concentration. Final beaker concentrations of 250 μM AA, 20, 40, and 60 μM L-glutamate, 2 μM DA, and 8.8 μM H_2O_2 were used to assess MEA performance. A total of 49 MEAs were used in the present study. The average ± standard error of the mean (SEM) for glutamate sensitivity was 5.7 ± 0.3 pA/μM (R^2 = 0.998 ± 0.001), selectivity ratio of 367 ± 48 to 1, and limit of detection of 0.20 ± 0.03 μM based on a signal-to-noise ratio of 3.

In Vivo Anesthetized Recordings:

A glass micropipette (World Precision Instruments, Inc.; Cat: 1B100–6) was used for local application studies. The tip of the micropipette (12–15 μm internal diameter) was positioned between the pair of recording sites and mounted ~100 μm above the MEA surface. Mice were anesthetized using 1.5% isoflurane (Henry Schein; Cat: 029405) in a calibrated vaporizer (Parkland Scientific; V3000) and placed in a stereotaxic frame with a mouse anesthesia mask (David Kopf Instruments; Cat: 900 / 907) with a mouse anesthesia mask. Body temperature was maintained at 37°C. The MEA / micropipette assembly was lowered into the dentate gyrus (DG; AP: −2.0, ML: ± 1.0, DV: −2.2 mm), CA3 (AP: −2.0, ML: ± 2.0, DV: −2.2 mm) and CA1 (AP: −2.0, ML: ± 1.0, DV: −1.7 mm) from Bregma (Paxinos and Franklin 2004). A Ag/AgCl reference wire was positioned beneath the skull and rostral to the right hemisphere craniotomy. Constant voltage amperometry (4Hz) was performed using the FAST16mkIII. Calibration data, in conjunction with a MATLAB (MathWorks, Natick, MA; RRID:SCR_014289) graphic user interface program (Version 6.1) was used to calculate extracellular glutamate. The sentinel site current (pA) was subtracted from the glutamate recording site current (pA) and divided by the slope (pA/μM) obtained during the calibration (Burmeister and Gerhardt 2001; Burmeister *et al.* 2002; Hascup *et al.* 2010; Hascup *et al.* 2011).

Immunohistochemistry & Semi-Quantification:

Following *in vivo* electrochemistry, the brains were removed and post-fixed in 4% paraformaldehyde for 48 hours and then transferred into 30% sucrose in 0.1M PB for 24 hours prior to sectioning. Forty-five micron sections of the hippocampus were obtained using a Microm cryostat (Zeiss; Cat: HM 500). Serial sections (every 6^{th}) of the hippocampus were processed for free-floating immunohistochemistry (IHC) using rabbit

polyclonal GFAP (1:2,000) or guinea pig polyclonal VGLUT1 antibody (1:1,000) (Farrand *et al.* 2017; Hascup *et al.* 2016). Endogenous peroxidase activity was quenched by treating sections with 10% H_2O_2 in 20% methanol for 10 minutes. Sections for primary antibodies were permeabilized in Tris-buffered saline with 0.25% TritonX-100 following treatment for 20 minutes with sodium metaperiodate. Nonspecific binding was controlled by 1 hour incubation in 10% normal goat serum. Sections were incubated overnight in the primary antibody at room temperature. The next day, sections were incubated for 1 hour with the secondary antibody (1:200; biotinylated goat anti-rabbit serum or biotinylated goat anti-guinea pig serum) and 1 hour with the Vectastain ABC kit (Vector). The reaction was developed using the VIP peroxidase substrate kit (Vector) to enhance the reaction and produce a color stain. This reaction was stopped using 0.1 M PB, and the sections were mounted on glass slides, dehydrated, and cover-slipped with DPX. To control for staining intensity, staining of all sections for each antibody was conducted on the same day and developed with VIP for the same amount of time (GFAP: 3 minutes, VGLUT1: 2 minutes). For plaque staining, slides containing serial sections (every 6^{th}) of the hippocampus were incubated for 10 min in freshly prepared Amylo-Glo® RTD™ solution followed by a 5 min rinse in 0.9% saline without shaking, then 1 minute incubation with EtBr based on product protocol (1:100). Staining intensities of GFAP, VGLUT1, and plaque formation in the hippocampus were determined using National Institutes of Health Image J Software 1.48 (RRID:SCR_003070) to measure a gray scale value within the range of 0–256, where 0 represents white and 256 represents black (Farrand *et al.* 2017). A template for the DG, CA3, and CA1 hippocampal subregions for VGLUT1 and GFAP while a template for the whole hippocampus was created for plaque formation. Templates were used on all brains similarly, and images were captured with a Nikon Eclipse E-600 microscope equipped with an Olympus-750 video camera system, and a Dell Pentium III computer. Measurements were performed blinded, and approximately six sections were averaged to obtain one value per subject. If six sections per stain were not obtained, the subject was excluded from data analysis. Staining density was obtained when background staining was subtracted from mean staining intensities on every sixth section through the hippocampus.

$A\beta_{42}$ ELISA:

A separate cohort of mice were used for insoluble $A\beta_{42}$ determination. Mice were euthanized as described above and the hippocampus was dissected and stored at −80°C until tissue processing. Protein concentrations were determined using the BCA method and assessment of the insoluble fractions of $A\beta_{42}$ were performed using the Human / Rat β amyloid (42) ELISA kit (WAKO Chemicals; Cat: 292–64501).

Data Analysis:

Sample size was determined based on previous MWM, electrochemical, and IHC data using C57BL/6J and AβPP/PS1 mice. A power calculation indicated a minimum of 10 mice per group for MWM and electrochemical recordings and 5 mice per group for IHC analysis (Boger *et al.* 2007, Hascup & Hascup, 2015) to detect differences with 95% confidence (α=0.05) and 0.8 power. Prism (GraphPad Software, Inc., La Jolla, CA; RRID:SCR_002798) software was used for all statistical analyses including D'Agostino-Pearson omnibus normality tests. A one-way Analysis of Variance (ANOVA) was used for

MWM and for electrochemical stimulus volume comparisons, while a two-way ANOVA (diet vs genotype) was used for all other analyses. When the ANOVA indicated a statistically significant main effect, a Holm-Sidak's multiple comparisons post-hoc test was used. Outliers were determined with a single Grubb's test (α=0.05). Data are represented as mean ± SEM and significance was defined as $p<0.05$. The unit of analysis "n" for each data set refers to the number of mice and data is available upon request.

Results

Changes in weight gain induced by a HFD:

An outline of the experimental design is presented in Figure 1A. All mice were given a two week acclimation period when they arrived at our animal facility, placed on standard chow for 2 weeks, and weighed weekly until study completion (Figure 1B). Following the two week acclimation period, pseudo randomization was used to assign mice to either the C57BL/6J LFD (n=14), C57BL/6J HFD (n=11), AβPP/PS1 LFD (n=11), or AβPP/PS1 HFD (n=12) groups. All mice remained on their respective diets until study completion. A diet effect was observed by four weeks ($F[3,44] = 81.29$; $P<0.0001$). As expected, both C57BL/6J and AβPP/PS1 mice on HFD gained more weight compared to genotype matched LFD groups No differences in weight gain were observed between genotypes within each diet group.

HFD impairs peripheral insulin sensitivity:

After 24 weeks on their respective diets, the effects of a HFD on the sensitivity of blood glucose levels to the action of insulin were tested with an ipITT. No difference in blood glucose levels were observed during a four hour fast (Figure 1C). A HFD significantly impaired peripheral insulin sensitivity compared to genotype matched LFD mice when examining the 120 minute blood glucose response to the insulin challenge ($F[3,44] = 23.58$; $P<0.0001$; Figure 1D) as well as the subsequent area under the curve analysis ($F[1,44] = 45.41$; $P<0.0001$; Figure 1E) indicating an obesity-induced T2DM phenotype. Additionally, an effect of genotype ($F[1,44] = 15.61$; $P=0.0003$) was observed supporting that AβPP/PS1 mice have impaired insulin sensitivity that is independent of diet (Figure 1D-E).

Glucose metabolism is impaired in mice fed a HFD:

The effects of a HFD on glucose metabolism was tested using the ipGTT. Mice fed a HFD had significantly ($F[1,44] = 42.28$; $P<0.0001$; Figure 1F) elevated 15 hour fasting blood glucose compared to genotype matched LFD mice as a result of the obesity-induced insulin resistance. Mice fed a HFD metabolized glucose slower during the 120 minute glucose challenge ($F[3,44] = 8.019$; $P=0.0002$) and subsequent area under the curve analysis ($F[1,44] = 18.32$; $P<0.0001$) compared to genotype matched LFD mice (Figure 1G-H).

Mice on a HFD have impaired spatial learning and memory:

One week following ipGTT and 27 weeks into dietary feeding, mice underwent a 3 day MWM. The MWM tests spatial learning and memory recall by requiring the mouse to utilize visual cues to repeatedly swim to a static, submerged platform, regardless of the starting quadrant. During the MWM, mice were trained to locate a visible escape platform on Day 1

and a hidden platform on Day 2. The visible platform verifies visual acuity while simultaneously habituating the mice to the novel environment thereby reducing stress while encouraging a motivation to escape the pool (Gulinello *et al.* 2009). The three training sessions for Day 1 and for each training block in Day 2 were averaged for individual mice for analysis. Latency to reach to the platform as well as cumulative distance from the platform were assessed. Cumulative distance is a proximity measure designed to reflect search error through summation of the distance from the platform calculated at one second intervals while accounting for trial variations in starting quadrant and swimming speed (Gallagher *et al.* 2015). As shown in Figure 2A, AβPP/PS1 HFD took longer to locate the hidden escape platform during the first training block of Day 2 compared to their Day 1 performance ($F[3,44] = 4.118$; $P=0.0117$). In Figure 2B, C57BL/6J LFD mice were the only group that did not travel further from the hidden escape platform on the first training block of Day 2 and continued to significantly decrease over successive training blocks ($F[3,52] = 3.449$; $P=0.0231$) compared to their Day 1 performance. On the contrary, the other three groups of mice traveled further from the hidden escape platform on the first training block of Day 2, which was significant in AβPP/PS1 HFD mice ($F[3,44] = 5.178$; $P=0.0038$) compared to their Day 1 performance. While C57BL/6J HFD and both AβPP/PS1 diet groups decreased the cumulative distance from the hidden escape platform over successive training blocks, a significant improvement over Day 1 performance was not observed supporting decreased learning in these three groups of mice. During the MWM probe challenge for memory recall, no differences were observed in the number of annulus 40 crossings (Figure 2C).

HFD elevates hippocampal basal glutamate:

A minimum of 2 weeks post MWM (29 weeks into dietary feeding) an enzyme based MEA was used to measure glutamate dynamics in the DG, CA3, and CA1. Representative glutamate traces showing basal and stimulus-evoked glutamate release are presented in Figure 3. Basal glutamate was calculated by taking a 10 s baseline average prior to start of pressure ejection in the DG, CA3, and CA1. When examining basal glutamate (Figures 4A-C), a genotype effect was only observed in the CA1 ($F[1,43] = 12.23$; $P=0.0011$), indicating increased tonic glutamate in AβPP/PS1 mice. A diet effect was observed in the DG ($F[1,43] = 6.232$; $P=0.0165$), CA3 ($F[1,43] = 12.90$; $P=0.0008$), and CA1 ($F[1,43] = 12.78$; $P=0.0009$), supporting that a HFD elevates basal glutamate with synergistic effects observed in AβPP/PS1 mice.

HFD alters hippocampal glutamate dynamics:

A glass micropipette attached to the enzyme-based MEA was used to locally apply sterile filtered (0.20 μm) 70 mM KCl (70 mM KCl, 79 mM NaCl and 2.5 mM $CaCl_2$, pH 7.4) by pressure ejection (5–15 psi, 1–2 s pulses) using a Picospritzer III (Parker-Hannafin Corp.). Ejection volumes were maintained between 100–200 nl in each hippocampal subfield and monitored using a stereomicroscope (Luxo Corp. Cat:, Elmsford, NY) fitted with a calibrated reticule (Hascup and Hascup 2016). Similar volumes of stimulus were locally applied in the DG ($F[3,40] = 0.7720$; $P=0.5165$), CA3 ($F[3,40] = 0.3397$; $P=0.7967$), and CA1 ($F[3,41] = 1.655$; $P=0.1915$) of all mouse groups to elicit glutamate release (Figures 4D-F). A genotype effect was observed in the DG ($F[1,40] = 8.429$; $P=0.0060$), CA3

(F[1,40] = 4.720; P=0.0358), and CA1 (F[1,41] = 7.559; P=0.0088), whereby AβPP/PS1 mice release more glutamate upon depolarization. A diet effect was observed in the DG (F[1,40] = 12.57 P = 0.0010) and CA1 (F[1,41] = 5.772; P=0.0209), but not the CA3 (F[1,40] = 0.0870; P=0.7695), indicating a HFD increased stimulus-evoked glutamate release. The clearance of glutamate is predominantly mediated by uptake in high-efficiency excitatory amino acid transporters (EAAT) located on glia (Zhou and Danbolt 2013). A significant effect of genotype was observed for glutamate uptake rate in the DG (F[1,42] = 6.050; P=0.0181) and CA3 (F[1,42] = 5.793; P = 0.0206), but not the CA1 (Figures 4G-I). A significant effect from diet led to increased glutamate uptake rate only in the CA1 (F[1,40] = 5.721; P=0.0216).

Increased expression of VGLUT1 in HFD mice:

IHC was used to determine changes in VGLUT1 expression in the DG, CA3, and CA1. Representative images of VGLUT1 from the DG are shown in Figures 5A-D (40x magnification) and average mean density for each hippocampal subfield are presented in Figures 5E-G. A significant effect of genotype on VGLUT1 expression was observed in the DG (F[1,34] = 12.40; P=0.0012), CA3 (F[1,33] = 12.59; P=0.0012) and CA1 (F[1,36] = 32.74; P<0.0001), supporting that the elevated hippocampal basal and stimulus-evoked glutamate release in APP/PS1 mice is a result of increased glutamatergic vesicles. Likewise, a significant effect of diet existed on VGLUT1 expression in the DG (F[1,34] = 17.67; P=0.0002), CA3 (F[1,33] = 27.63; P<0.0001) and CA1 (F[1,36] = 17.54; P=0.0002), indicating that a HFD increased glutamatergic vesicles corresponding with the elevated hippocampal glutamate.

GFAP expression is increased by HFD:

IHC was used to determine changes in GFAP expression in the DG, CA3, and CA1. Whole hippocampal representative images (10x magnification) of GFAP expression are shown in Figures 6A-D and average mean density for each hippocampal subfield are presented in Figures 6E-G. A significant effect of genotype on GFAP expression was observed in the DG (F[1,36] = 14.83; P = 0.0005), CA3 (F[1,37] = 23.07; P<0.0001), and CA1 (F[1,39] = 100.60; P<0.0001), as indicated by greater hippocampal GFAP expression in APP/PS1 mice. In addition, a significant effect of diet exists on GFAP expression in the C57BL/6J DG (F[1,36] = 9.006; P=0.0049) and AβPP/PS1 CA3 (F[1,37] = 20.13; P<0.0001) and CA1 (F[1,39] = 15.98; P=0.0003), indicating that a HFD results in greater astrogliosis.

A HFD does not alter plaque formation:

Hippocampal plaque formation was determined by staining with Amylo-Glo® RTD™. Whole hippocampal representative images (10x magnification) of plaque accumulation (blue) and EtBr counter stain (red) are shown in Figures 7A-D and average mean density of whole hippocampal plaque accumulation is presented in Figure 7E. As indicated by the arrows in Figures 7C and 7D, a genotype effect caused increased plaque accumulation (F[1,16] = 1410.0; P<0.0001). However, a diet effect was not observed (F[1,16] = 0.1096; P=0.7449), indicating that a HFD does not increase plaque deposition in AβPP/PS1 mice. This was further supported by ELISA determination in a separate cohort of mice showing a

genotype effect (F[1,24] = 49.95; P<0.0001), but not a diet effect (F[1,24] = 0.79; P=0.3828).

Discussion

Half of AD cases are attributable to modifiable lifestyle factors (Barnes and Yaffe 2011) including obesity-induced T2DM that has been suggested to increase the risk for developing AD 1.5- to 2-fold (Allen *et al.* 2004; Ott *et al.* 1999; Arvanitakis *et al.* 2004). While the exact molecular events linking T2DM to AD have not been fully elucidated, the metabolic hypothesis of AD (Hoyer 2002) supports impaired insulin signaling initiates a series of events including, Aβ accumulation (Farris *et al.* 2003), neuroinflammation (Granic *et al.* 2009), oxidative stress (De Felice and Ferreira 2014) and calcium dyshomeostasis (Zhang *et al.* 2017) leading to AD pathogenesis. The results of the present study support addition of elevated hippocampal glutamatergic signaling to this growing body of molecular parallels.

In the present study, starting at 3 months of age C57BL/6J and AβPP/PS1 mice were placed on either LFD (10% kcal from fat) or HFD (60% kcal from fat) with matching protein and sucrose content. Mice fed a HFD developed an obese phenotype starting one month after diet initiation and continued until study completion. Since insulin sensitivity is positively correlated to increased longevity and healthspan in vertebrates (Arum *et al.* 2014) we choose to examine peripheral blood glucose clearance in these mice. The obese phenotype resulted in impaired peripheral insulin signaling and glucose tolerance as observed in the ipITT and ipGTT. The insulin resistance observed in the HFD mouse groups explains the elevated 15 hr fasting blood glucose levels compared to genotype matched LFD groups. Interestingly, AβPP/PS1 mice fed a LFD had a similar metabolic profile to HFD mice supporting a naturally occurring insulin resistance in these mice, which has been reported elsewhere (Pedrós *et al.* 2014; Macklin *et al.* 2017). Despite the innate insulin resistance observed in AβPP/PS1 mice, HFD led to a further disruption of their metabolic profile.

A HFD has been shown to negatively affect learning and memory in cognitively normal rodents (Kanoski and Davidson 2011; Cordner and Tamashiro 2015) as well as exacerbate cognitive decline and AD-related neuropathology in animal models (Vandal *et al.* 2014; Knight *et al.* 2014; Thériault *et al.* 2016; Julien *et al.* 2010). For this study, diet treatments began prior to the onset of typically reported AD-related pathology and continued through an age when pathology and plaque burden are well developed in the AβPP/PS1 mouse model. During the visible portion (Day 1) of the MWM behavioral task, similar performances in the latency to the platform and cumulative distance traveled from the platform were observed in all groups of mice, indicating comparable visual acuity and physical activity despite weight differences. Learning impairments in AβPP/PS1 mice were discerned during the second training day with the hidden escape platform. Throughout the training blocks, we observed a higher percentage of C57BL/6J LFD and HFD mice successfully navigate the MWM while traveling less distance from the platform. To the contrary, AβPP/PS1 mice presented with learning impairments that were worsened when fed a HFD as supported by 1) a slower escape latency and 2) the cumulative distance from the submerged escape platform during the first two training blocks. By the third training block, AβPP/PS1 performance was similar to that observed during the Day 1 visible platform, but

no significant improvements were observed. However, during the MWM probe challenge on the third day, no differences in the number of annulus 40 crossing was observed. The MWM paradigm employed in this study, while atypical from previously published reports from our laboratory (Hascup and Hascup 2015), was designed to reduce stress and anxiety in the mouse. The visible platform on Day 1 helped to habituate mice to the novel pool environment while testing for visual acuity since some inbred mouse strains develop retinal degeneration (Chang *et al.* 2002). Furthermore, the shorter training duration avoided learning limitations from multiple practice sessions, prevented fatigue, and increased throughput (Alamed *et al.* 2006). These data support that a HFD can negatively affect learning in both C57BL/6J and AβPP/PS1 mice.

Glutamate, the predominant excitatory neurotransmitter in the mammalian CNS, plays an essential role in learning and memory (Riedel *et al.* 2003) and has been implicated in several neurodegenerative disorders including Huntington's, Parkinson's, and Alzheimer's diseases. To measure glutamate, we used an enzyme-based MEA with high spatial resolution (50 × 100 μm recording sites) that allowed for independent measures from the DG, CA3, and CA1 dorsal hippocampus, a region that is important for consolidation and retrieval of spatial memory during the MWM task (Cimadevilla *et al.* 2005). In the present study, AβPP/PS1 LFD mice exhibited elevated basal glutamate (CA1) and stimulus-evoked glutamate release (DG, CA3, and CA1) compared to C57BL/6J LFD mice. The elevated basal glutamate may result from a combination of mechanisms affecting soluble $A\beta_{42}$ levels that are known to elicit glutamate release (Hascup and Hascup 2016; Talantova *et al.* 2013). First, the transgene expressions in AβPP/PS1 result in progressive $A\beta_{42}$ accumulation (Alley *et al.* 2010), and second, the insulin resistance observed in these mice may prevent IDE from degrading monomeric $A\beta_{42}$ leading to further accumulation and overactivation of α7nAChR on presynaptic glutamatergic terminals. Since hippocampal tissue were used for IHC, none was available for biochemical analysis. Further studies examining soluble $A\beta_{42}$ are needed in order to validate this hypothesis.

VGLUT1, the predominant subtype of vesicles that store hippocampal glutamate (Liguz-Lecznar and Skangiel-Kramska, 2007), was increased in the CA3 and CA1 of AβPP/PS1 LFD compared to C57BL/6J LFD mice. Increased expression of VGLUT1 has been demonstrated to cause excess glutamate release (Daniels *et al.* 2011), however, homeostatic mechanisms exist to limit aberrant synaptic firing that may arise from environmental or genetic variations. But, during the early stages of AD, it is hypothesized that these negative feedback mechanisms begin to destabilize in cortical and hippocampal regions (Frere and Slutsky 2018). For example, epileptiform spikes have been observed in both AβPP/PS1 mice (Minkeviciene *et al.* 2009) and amnestic mild cognitively impaired patients (Vossel *et al.* 2013) as well as hyperexcitability of CA1 pyramidal neurons in AβPP/PS1 mice (Šišková *et al.* 2014). This hyperexcitability coupled with the increased VGLUT1 expression may explain the increased stimulus-evoked glutamate release observed throughout the hippocampus of the present study.

Both C57BL/6J and AβPP/PS1 mice fed a HFD presented with elevated basal (CA3 and CA1) and stimulus-evoked glutamate release (DG and CA1) compared to genotype-matched LFD mice. As described above, the increased extracellular glutamate observed in AβPP/PS1

HFD mice may be explained by the accumulation of $A\beta_{42}$ stimulating glutamate release, but this would not be the case in C57BL/6J HFD mice. However, a HFD would initiate a cascade of separate events in both genotypes leading to the increased basal and stimulus-evoked glutamate release. The insulin resistance and subsequent increase in circulating blood glucose levels observed in both HFD mice would lead to an increase in neuronal glucose accumulation. Since neuronal glutamate synthesis can be derived from glucose (Sonnewald 2014) the higher blood glucose levels would increase the neurotransmitter pool of glutamate, which is supported by the elevated VGLUT1 density observed in the DG, CA3, and CA1 of HFD mice.

A HFD can upregulate glial glutamate transporter expression while increasing the maximal velocity of clearance (Valladolid-Acebes *et al.* 2012). While the present study did not examine EAAT density, increased expression of GFAP is indicative of astrogliosis (Brahmachari *et al.* 2006) that is associated with an increase in glial glutamate transporters in response to chronic cerebral injuries and neurodegenerative disorders (Haroon *et al.* 2017). At first, this appears counterintuitive. More transporters supports faster glutamate clearance that would decrease basal and evoked glutamate concentrations. But, elevated glutamate release causes increased EAAT density as a mechanism to prevent chronic accumulation of extracellular glutamate and potential excitotoxicity (Munir *et al.* 2000). Although not significant in all hippocampal subregions, stimulus-evoked glutamate uptake was increased in AβPP/PS1 LFD vs diet-matched C57BL/6J mice and a HFD further increased these rates in the DG and CA3. In other words, glutamate uptake rate generally increased in response to increases in basal and stimulus-evoked glutamate release.

As expected, hippocampal plaque pathology was only observed in AβPP/PS1 mice, however, a HFD did not increase plaque density which is similar to previous reports in these mice (Thériault *et al.* 2016). This may be due to the astrogliotic response to control plaque deposition in the pathogenesis of AD (Kraft *et al.* 2013). As such, we observed increased hippocampal GFAP density in AβPP/PS1 LFD and HFD compared to diet-matched C57BL/6J control mice that did not present with plaque pathology. GFAP density throughout the hippocampus was further elevated in AβPP/PS1 HFD compared to LFD mice, but this was only mildly observed in the DG of C57BL/6J HFD mice. Since astroglia play a role in Aβ clearance (Ries and Sastre 2016), the elevated astrogliotic inflammatory response, particularly in AβPP/PS1 HFD mice may have prevented additional plaque accumulation.

The elevated extracellular hippocampal glutamate levels observed in C57BL/6J HFD as well as AβPP/PS1 LFD and HFD mice would contribute to their decreased performance on the MWM task reported here and elsewhere (Thériault *et al.* 2016). The NMDA receptor is important for spatial learning and memory tasks (Morris *et al.* 1986), but mild, chronic overactivation would be detrimental to synaptic plasticity. This argument is based on the signal-to-noise hypothesis of NMDA receptor activation. Elevated tonic glutamate levels (as observed in this study) prevents detection of phasic signals thereby blocking formation of new learning (Parsons *et al.* 2007). This process could occur over an extended period of time before calcium overload, excitotoxicity, and eventual neurodegeneration as observed in AD. As such, this mechanism helps to explain the cognitive-improving effects of memantine, an

NMDA receptor antagonist, in some AD patients (Parsons *et al.* 2007). In support of this, AβPP/PS1 mice fed a HFD followed by treatment with memantine saw significant reductions in insulin resistance, neuroinflammation, and cognitive deficits (Ettcheto *et al.* 2018). Alternatively, a HFD has been shown to decrease NMDA receptor subunit GluN2B leading to desensitization that may account for cognitive deficits (Valladolid-Acebes *et al.* 2012).

The concentration of extracellular basal glutamate is debated throughout the scientific literature with reports ranging from nanomolar to micromolar concentrations (Herman and Jahr 2007; Burmeister *et al.* 2013; Messam *et al.* 1995). These discrepancies are frequently attributed to methodological considerations that often times yield similar results when additional factors are taken into consideration. The size of our MEA recording sites limits our recording capabilities to the extracellular matrix (ECM) where we are measuring glutamate release and clearance from multiple synapses. As such, a summation of multiple extrasynaptic spillover events may cause elevated levels compared to those reported using patch clamp techniques in slice preparations. Additionally, the diffusion capabilities of neurotransmitters and other membrane impermeable molecules in the ECM are subject to both volume fraction ($\alpha = 0.2$) and tortuosity ($\lambda = 1.6$) (Syková and Nicholson 2008). The α effectively amplifies the concentration of extrasynaptic spillover of glutamate in the ECM while the λ simultaneously slows down its diffusion and uptake into high-affinity transporters. Furthermore, the depolarizing stimulus used in the present study creates a positive net charge on the ECM resulting in a drag effect on the negatively charged glutamate molecules (Gundelfinger *et al.* 2010), and changes the membrane potential which EAATs rely upon for efficient uptake of glutamate (Takahashi *et al.* 1997). The net effect is a slower clearance of stimulus-evoked glutamate release when compared to other methods. Of course, tissue damage is always a concern with any invasive technique including, but not limited to, slice preparations, microdialysis, and MEA recordings. However, the ceramic substrate (Al_2O_3) on the MEAs used in this study have good biocompatibility helping to limit CNS damage allowing for single-unit neuronal activity measurements for at least 6 months post-implantation (Hascup *et al.* 2009). The MEAs employed in this study have routinely demonstrated that basal extracellular glutamate are sensitive to Na^+-channel (tetrodotoxin), Ca^{2+}-channel (ω-conotoxin) and EAAT (DL-*threo*-β-Benzyloxyaspartic acid) blockade lending credence to a healthy parenchyma surrounding the implanted MEA (Hascup *et al.* 2010; Hascup and Hascup 2016; Hascup *et al.* 2007). Furthermore, the extracellular glutamate concentrations reported in this manuscript fall below the Km (~20 μM) for EAATs (Zhou and Danbolt 2013). And basal hippocampal glutamate concentrations for C57BL/6J LFD mice (~1 μM) are below the reported EC_{50} (3.7 μM) for the NR1/NR2B NMDA receptor (Banke and Traynelis 2003), further strengthening our premise that chronic overactivation of NMDA receptors, as observed in the HFD and AβPP/PS1 groups would be detrimental to synaptic plasticity, cognition, and may lead to eventual neurodegeneration. Regardless, the current study was not designed to be a definitive assessment of basal glutamate concentrations. In fact, the level of basal glutamate is dependent upon a number of criteria including transporter density (Herman and Jahr 2007), ECM developmental stage (Gundelfinger *et al.* 2010) and the glia-neuron ratio (Azevedo *et al.* 2009) resulting in marked variation between brain regions, maturation, and species (Burmeister *et al.* 2013).

Conclusion

Excitotoxicity is a proposed mechanism underlying the neurodegeneration associated with AD. However, the basal and stimulus-evoked glutamate release values reported here are not considered neurotoxic for an intact nervous system. Rather, the current study (when combined with previous research from our laboratory) highlights a consistent theme of elevated hippocampal glutamate starting as early as 2–4 months in AβPP/PS1 mice (Hascup and Hascup 2015) that is potentially mediated by soluble $A\beta_{42}$ (Hascup and Hascup 2016). Furthermore, obesity-induced insulin resistance caused cognitive impairments and increased extracellular glutamate in AβPP/PS1 mice. The progressive deposition of $A\beta_{42}$ with AD progression may chronically elevate glutamate leading to the cognitive and function decline observed in AD, which can be exacerbated by modifiable life-style factors such as obesity-induced insulin resistance. While additional studies are ongoing to elucidate mechanisms associated with dietary influences on glutamate dynamics in AβPP/PS1 mice, hippocampal glutamate levels may serve as a viable early therapeutic biomarker for AD pathogenesis.

Acknowledgments

Funding

This work was supported by NIH R01 AG057767, NIH R01 AG061937, Center for Alzheimer's Disease and Related Disorders at Southern Illinois University School of Medicine, the Kenneth Stark Endowment, and the Fraternal Order of Eagles (KNH, SOB, ERH), NIA AG051869 (YF, AB) and by the MUSC Barmore Foundation (MKR, HAB)

Abbreviations:

mPD	1,3 phenylenediamine dihydrochloride
α7nAChR	α7 nicotinic acetylcholine receptor
AD	Alzheimer's disease
AA	ascorbic acid
ANOVA	analysis of variance
ABC	avidin-biotin complex
Aβ	beta-amyloid
b.w.	body weight
BSA	bovine serum albumin
DG	dentate gyrus
DPX	dibutyl phthalate and xylene
DA	dopamine hydrochloride
EAAT	excitatory amino acid transporter

FAST	Fast Analytical Sensing Technology
GFAP	glial fibrillary acidic protein
GTT	glucose tolerance test
HFD	high-fat diet
IDE	insulin degrading enzyme
ITT	insulin tolerance test
ip	intraperitoneal
IHC	immunohistochemistry
LFD	low-fat diet
MEA	microelectrode array
MWM	Morris water maze
NMDA	N-methyl-D-aspartate
PBS	phosphate buffered saline
RRID	research resource identifiers
SEM	standard error of the mean
T2DM	Type 2 diabetes mellitus
VGLUT1	vesicular glutamate transporter 1

References

Alamed J, Wilcock DM, Diamond DM, Gordon MN, Morgan D (2006) Two-day radial-arm water maze learning and memory task; robust resolution of amyloid-related memory deficits in transgenic mice. Nat. Protoc 1, 1671–9. [PubMed: 17487150]

Allen KV, Frier BM, Strachan MWJ (2004) The relationship between type 2 diabetes and cognitive dysfunction: longitudinal studies and their methodological limitations. Eur. J. Pharmacol 490, 169–75. [PubMed: 15094083]

Alley GM, Bailey JA, Chen D, Ray B, Puli LK, Tanila H, Banerjee PK, Lahiri DK (2010) Memantine lowers amyloid-beta peptide levels in neuronal cultures and in APP/PS1 transgenic mice. J. Neurosci. Res 88, 143–54. [PubMed: 19642202]

Arum O, Boparai RK, Saleh JK, Wang F, Dirks AL, Turner JG, Kopchick JJ, Liu J-L, Khardori RK, Bartke A (2014) Specific suppression of insulin sensitivity in growth hormone receptor gene-disrupted (GHR-KO) mice attenuates phenotypic features of slow aging. Aging Cell 13, 981–1000. [PubMed: 25244225]

Arvanitakis Z, Wilson RS, Bienias JL, Evans DA, Bennett DA (2004) Diabetes mellitus and risk of Alzheimer disease and decline in cognitive function. Arch. Neurol 61, 661–6. [PubMed: 15148141]

Azevedo FAC, Carvalho LRB, Grinberg LT, Farfel JM, Ferretti REL, Leite REP, Jacob Filho W, Lent R, Herculano-Houzel S (2009) Equal numbers of neuronal and nonneuronal cells make the human brain an isometrically scaled-up primate brain. J. Comp. Neurol 513, 532–41. [PubMed: 19226510]

Banke TG, Traynelis SF (2003) Activation of NR1/NR2B NMDA receptors. Nat. Neurosci 6, 144–152. [PubMed: 12524545]

Barnes DE, Yaffe K (2011) The projected effect of risk factor reduction on Alzheimer's disease prevalence. Lancet. Neurol 10, 819–28. [PubMed: 21775213]

Boger HA, Middaugh LD, Patrick KS, Ramamoorthy S, Denehy ED, Zhu H, Pacchioni AM, Granholm A-C, McGinty JF (2007) Long-term consequences of methamphetamine exposure in young adults are exacerbated in glial cell line-derived neurotrophic factor heterozygous mice. J. Neurosci 27, 8816–25. [PubMed: 17699663]

Brahmachari S, Fung YK, Pahan K (2006) Induction of glial fibrillary acidic protein expression in astrocytes by nitric oxide. J. Neurosci 26, 4930–9. [PubMed: 16672668]

Burmeister JJ, Davis VA, Quintero JE, Pomerleau F, Huettl P, Gerhardt GA (2013) Glutaraldehyde cross-linked glutamate oxidase coated microelectrode arrays: selectivity and resting levels of glutamate in the CNS. ACS Chem. Neurosci 4, 721–8. [PubMed: 23650904]

Burmeister JJ, Gerhardt GA (2001) Self-referencing ceramic-based multisite microelectrodes for the detection and elimination of interferences from the measurement of L-glutamate and other analytes. Anal. Chem 73, 1037–42. [PubMed: 11289414]

Burmeister JJ, Moxon K, Gerhardt GA (2000) Ceramic-based multisite microelectrodes for electrochemical recordings. Anal. Chem 72, 187–92. [PubMed: 10655652]

Burmeister JJ, Pomerleau F, Palmer M, Day BK, Huettl P, Gerhardt GA (2002) Improved ceramic-based multisite microelectrode for rapid measurements of L-glutamate in the CNS. J. Neurosci. Methods 119, 163–71. [PubMed: 12323420]

Chang B, Hawes NL, Hurd RE, Davisson MT, Nusinowitz S, Heckenlively JR (2002) Retinal degeneration mutants in the mouse. Vision Res 42, 517–525. [PubMed: 11853768]

Cimadevilla JM, Miranda R, López L, Arias JL (2005) Partial unilateral inactivation of the dorsal hippocampus impairs spatial memory in the MWM. Brain Res. Cogn. Brain Res 25, 741–6. [PubMed: 16216479]

Cordner ZA, Tamashiro KLK (2015) Effects of high-fat diet exposure on learning & memory. Physiol. Behav 152, 363–371. [PubMed: 26066731]

Cummings JL, Morstorf T, Zhong K (2014) Alzheimer's disease drug-development pipeline: few candidates, frequent failures. Alzheimers. Res. Ther 6, 37. [PubMed: 25024750]

Daniels RW, Miller BR, DiAntonio A (2011) Increased vesicular glutamate transporter expression causes excitotoxic neurodegeneration. Neurobiol. Dis 41, 415–20. [PubMed: 20951206]

Ettcheto M, Sánchez-López E, Gómez-Mínguez Y, Cabrera H, Busquets O, Beas-Zarate C, García ML, et al. (2018) Peripheral and Central Effects of Memantine in a Mixed Preclinical Mice Model of Obesity and Familial Alzheimer's Disease. Mol. Neurobiol 55, 7327–7339. [PubMed: 29404958]

Fang Y, McFadden S, Darcy J, Hill CM, Huber JA, Verhulst S, Kopchick JJ, Miller RA, Sun LY, Bartke A (2017) Differential effects of early-life nutrient restriction in long-lived GHR-KO and normal mice. GeroScience 39, 347–356. [PubMed: 28523599]

Farrand AQ, Helke KL, Gregory RA, Gooz M, Hinson VK, Boger HA (2017) Vagus nerve stimulation improves locomotion and neuronal populations in a model of Parkinson's disease. Brain Stimul 10, 1045–1054. [PubMed: 28918943]

Farris W, Mansourian S, Chang Y, Lindsley L, Eckman EA, Frosch MP, Eckman CB, Tanzi RE, Selkoe DJ, Gue S (2003) Insulin-degrading enzyme regulates the levels of insulin, amyloid beta-protein, and the beta amyloid precursor protein intracellular domain in vivo 100, 4162–7.

De Felice F. G. (2013) Alzheimer's disease and insulin resistance: translating basic science into clinical applications. J. Clin. Invest 123, 531–9. [PubMed: 23485579]

De Felice F. G., Ferreira ST. (2014) Inflammation, defective insulin signaling, and mitochondrial dysfunction as common molecular denominators connecting type 2 diabetes to Alzheimer disease. Diabetes 63, 2262–72. [PubMed: 24931033]

Frere S, Slutsky I (2018) Alzheimer's Disease: From Firing Instability to Homeostasis Network Collapse. Neuron 97, 32–58. [PubMed: 29301104]

Gallagher M, Burwell R, Burchinal M (2015) Severity of spatial learning impairment in aging: Development of a learning index for performance in the Morris water maze. Behav. Neurosci 129, 540–8. [PubMed: 26214219]

Godyń J, Jończyk J, Panek D, Barbara M (2016) Therapeutic strategies for Alzheimer's disease in clinical trials. Pharmacol. Reports 68, 127–138.

Granic I, Dolga AM, Nijholt IM, Dijk G. van, Eisel ULM (2009) Inflammation and NF-κB in Alzheimer's Disease and Diabetes. J. Alzheimer's Dis 16, 809–821. [PubMed: 19387114]

Gulinello M, Gertner M, Mendoza G, Schoenfeld BP, Oddo S, LaFerla F, Choi CH, McBride SMJ, Faber DS (2009) Validation of a 2-day water maze protocol in mice. Behav. Brain Res 196, 220–227. [PubMed: 18831990]

Gundelfinger ED, Frischknecht R, Choquet D, Heine M (2010) Converting juvenile into adult plasticity: a role for the brain's extracellular matrix. Eur. J. Neurosci 31, 2156–2165. [PubMed: 20497467]

Haroon E, Miller AH, Sanacora G (2017) Inflammation, Glutamate, and Glia: A Trio of Trouble in Mood Disorders. Neuropsychopharmacology 42, 193–215. [PubMed: 27629368]

Hascup KN, Hascup ER, Littrell OM, Hinzmann JM, Werner CE, Davis VA, Burmeister JJ, Pomerleau F, Quintero J, Huettl P, Gerhardt GA (2013) Microelectrode Array Fabrication and Optimization for Selective Neurochemical Detection, in Microelectrode Biosens, (Marinesco S, Dale N, eds), Vol. 80, pp. 27–54. Humana Press, Totowa, NJ.

Hascup ER, af Bjerkén S, Hascup KN, Pomerleau F, Huettl P, Strömberg I, Gerhardt GA (2009) Histological studies of the effects of chronic implantation of ceramic-based microelectrode arrays and microdialysis probes in rat prefrontal cortex. Brain Res 1291.

Hascup ER, Hascup KN, Stephens M, Pomerleau F, Huettl P, Gratton A, Gerhardt GA (2010) Rapid microelectrode measurements and the origin and regulation of extracellular glutamate in rat prefrontal cortex. J. Neurochem 115, 1608–1620. [PubMed: 20969570]

Hascup KN, Hascup ER (2015) Altered neurotransmission prior to cognitive decline in AβPP/PS1 mice, a model of Alzheimer's disease. J. Alzheimer's Dis 44, 771–776. [PubMed: 25374106]

Hascup KN, Hascup ER (2016) Soluble Amyloid-β42 Stimulates Glutamate Release through Activation of the α7 Nicotinic Acetylcholine Receptor. J. Alzheimer's Dis 53, 337–347. [PubMed: 27163813]

Hascup KN, Hascup ER, Pomerleau F, Huettl P, Gerhardt GA (2007) Second-by-Second Measures of L-Glutamate in the Prefrontal Cortex and Striatum of Freely Moving Mice. J. Pharmacol. Exp. Ther 324, 725–731. [PubMed: 18024788]

Hascup KN, Hascup ER, Stephens ML, Glaser PEA, Yoshitake T, Mathé AA, Gerhardt GA, Kehr J (2011) Resting glutamate levels and rapid glutamate transients in the prefrontal cortex of the Flinders Sensitive Line rat: a genetic rodent model of depression. Neuropsychopharmacology 36, 1769–1777. [PubMed: 21525860]

Hascup KN, Lynn MK, Fitzgerald PJ, Randall S, Kopchick JJ, Boger HA, Bartke A, Hascup ER (2016) Enhanced Cognition and Hypoglutamatergic Signaling in a Growth Hormone Receptor Knockout Mouse Model of Successful Aging. J. Gerontol. A. Biol. Sci. Med. Sci 72, 329–337.

Hascup KN, Rutherford EC, Quintero JE, Day BK, Nickell JR, Pomerleau F, Huettl P, Burmeister JJ, Gerhardt GA (2006) Second-by-Second Measures of L-Glutamate and Other Neurotransmitters Using Enzyme-Based Microelectrode Arrays - Electrochemical Methods for Neuroscience - NCBI Bookshelf, in Electrochem. Methods Neurosci, (Borland AC, Michael LM, eds), pp. 407–450. CRC Press.

Herman MA, Jahr CE (2007) Extracellular glutamate concentration in hippocampal slice. J. Neurosci 27, 9736–41. [PubMed: 17804634]

Holland WL, Brozinick JT, Wang L-P, Hawkins ED, Sargent KM, Liu Y, Narra K, et al. (2007) Inhibition of Ceramide Synthesis Ameliorates Glucocorticoid-, Saturated-Fat-, and Obesity-Induced Insulin Resistance. Cell Metab 5, 167–179. [PubMed: 17339025]

Hoyer S (2002) The brain insulin signal transduction system and sporadic (type II) Alzheimer disease: an update. J. Neural Transm 109, 341–360. [PubMed: 11956956]

Jack CR, Knopman DS, Jagust WJ, Petersen RC, Weiner MW, Aisen PS, Shaw LM, et al. (2013) Tracking pathophysiological processes in Alzheimer's disease: an updated hypothetical model of dynamic biomarkers. Lancet. Neurol 12, 207–16. [PubMed: 23332364]

Janson J, Laedtke T, Parisi JE, O'Brien P, Petersen RC, Butler PC (2004) Increased risk of type 2 diabetes in Alzheimer disease. Diabetes 53, 474–81. [PubMed: 14747300]

Jin M, Selkoe DJ (2015) Systematic analysis of time-dependent neural effects of soluble amyloid β oligomers in culture and in vivo: Prevention by scyllo-inositol. Neurobiol. Dis 82, 152–63. [PubMed: 26054438]

Julien C, Tremblay C, Phivilay A, Berthiaume L, Émond V, Julien P, Calon F (2010) High-fat diet aggravates amyloid-beta and tau pathologies in the 3xTg-AD mouse model. Neurobiol. Aging 31, 1516–1531. [PubMed: 18926603]

Kanoski SE, Davidson TL (2011) Western diet consumption and cognitive impairment: links to hippocampal dysfunction and obesity. Physiol. Behav 103, 59–68. [PubMed: 21167850]

Knight EM, Martins IVA, Gümüsgöz S, Allan SM, Lawrence CB (2014) High-fat diet-induced memory impairment in triple-transgenic Alzheimer's disease (3xTgAD) mice is independent of changes in amyloid and tau pathology. Neurobiol. Aging 35, 1821–32. [PubMed: 24630364]

Kraft AW, Hu X, Yoon H, Yan P, Xiao Q, Wang Y, Gil SC, et al. (2013) Attenuating astrocyte activation accelerates plaque pathogenesis in APP/PS1 mice. FASEB J 27, 187–98. [PubMed: 23038755]

Liguz-lecznar M, Skangiel-kramska J (2007) Vesicular glutamate transporters (VGLUTs): The three musketeers of glutamatergic system

Macklin L, Griffith CM, Cai Y, Rose GM, Yan X-X, Patrylo PR (2017) Glucose tolerance and insulin sensitivity are impaired in APP/PS1 transgenic mice prior to amyloid plaque pathogenesis and cognitive decline. Exp. Gerontol 88, 9–18. [PubMed: 28025127]

Messam CA, Greene JG, Greenamyre JT, Robinson MB (1995) Intrastriatal injections of the succinate dehydrogenase inhibitor, malonate, cause a rise in extracellular amino acids that is blocked by MK-801. Brain Res 684, 221–4. [PubMed: 7583227]

Minkeviciene R, Rheims S, Dobszay MB, Zilberter M, Hartikainen J, Fulop L, Penke B, et al. (2009) Amyloid -Induced Neuronal Hyperexcitability Triggers Progressive Epilepsy. J. Neurosci 29, 3453–3462. [PubMed: 19295151]

Moloney AM, Griffin RJ, Timmons S, O'Connor R, Ravid R, O'Neill C (2010) Defects in IGF-1 receptor, insulin receptor and IRS-1/2 in Alzheimer's disease indicate possible resistance to IGF-1 and insulin signalling. Neurobiol. Aging 31, 224–43. [PubMed: 18479783]

Morris RG, Anderson E, Lynch GS, Baudry M (1986) Selective impairment of learning and blockade of long-term potentiation by an N-methyl-D-aspartate receptor antagonist, AP5. Nature 319, 774–6. [PubMed: 2869411]

Mota SI, Ferreira IL, Rego AC (2014) Dysfunctional synapse in Alzheimer's disease – A focus on NMDA receptors. Neuropharmacology 76, 16–26. [PubMed: 23973316]

Munir M, Correale DM, Robinson MB (2000) Substrate-induced up-regulation of Na(+)-dependent glutamate transport activity. Neurochem. Int 37, 147–62. [PubMed: 10812200]

Ott A, Stolk RP, Harskamp F. van, Pols HA, Hofman A, Breteler MM (1999) Diabetes mellitus and the risk of dementia: The Rotterdam Study. Neurology 53, 1937–42. [PubMed: 10599761]

Parsons CG, Stöffler A, Danysz W (2007) Memantine: a NMDA receptor antagonist that improves memory by restoration of homeostasis in the glutamatergic system--too little activation is bad, too much is even worse. Neuropharmacology 53, 699–723. [PubMed: 17904591]

Paxinos G, Franklin KBJ (2004) The Mouse Brain in Stereotaxic Coordinates Gulf Professional Publishing.

Pedrós I, Petrov D, Allgaier M, Sureda F, Barroso E, Beas-Zarate C, Auladell C, et al. (2014) Early alterations in energy metabolism in the hippocampus of APPswe/PS1dE9 mouse model of Alzheimer's disease. Biochim. Biophys. Acta 1842, 1556–66. [PubMed: 24887203]

Riedel G, Platt B, Micheau J (2003) Glutamate receptor function in learning and memory. Behav. brain Res. brain Res 140, 1–47.

Ries M, Sastre M (2016) Mechanisms of Aβ Clearance and Degradation by Glial Cells. Front. Aging Neurosci 8, 160. [PubMed: 27458370]

Šišková Z, Justus D, Kaneko H, Friedrichs D, Henneberg N, Beutel T, Pitsch J, et al. (2014) Dendritic Structural Degeneration Is Functionally Linked to Cellular Hyperexcitability in a Mouse Model of Alzheimer's Disease. Neuron 84, 1023–1033. [PubMed: 25456500]

Sonnewald U (2014) Glutamate synthesis has to be matched by its degradation - where do all the carbons go? J. Neurochem 131, 399–406. [PubMed: 24989463]

Syková E, Nicholson C (2008) Diffusion in brain extracellular space. Physiol. Rev 88, 1277–340. [PubMed: 18923183]

Takahashi M, Billups B, Rossi D, Sarantis M, Hamann M, Attwell D (1997) The role of glutamate transporters in glutamate homeostasis in the brain. J. Exp. Biol 200, 401–409. [PubMed: 9050249]

Talantova M, Sanz-Blasco S, Zhang X, Xia P, Akhtar MW, Okamoto S, Dziewczapolski G, et al. (2013) Aβ induces astrocytic glutamate release, extrasynaptic NMDA receptor activation, and synaptic loss. Proc. Natl. Acad. Sci. U. S. A 110, E2518–27. [PubMed: 23776240]

Talbot K, Wang H-Y, Kazi H, Han L-Y, Bakshi KP, Stucky A, Fuino RL, et al. (2012) Demonstrated brain insulin resistance in Alzheimer's disease patients is associated with IGF-1 resistance, IRS-1 dysregulation, and cognitive decline. J. Clin. Invest 122, 1316–38. [PubMed: 22476197]

Thériault P, ElAli A, Rivest S (2016) High fat diet exacerbates Alzheimer's disease-related pathology in APPswe/PS1 mice. Oncotarget 7, 67808–67827. [PubMed: 27661129]

Valladolid-Acebes I, Merino B, Principato A, Fole A, Barbas C, Lorenzo MP, García A, et al. (2012) High-fat diets induce changes in hippocampal glutamate metabolism and neurotransmission. Am. J. Physiol. Endocrinol. Metab 302, E396–402. [PubMed: 22114023]

Vandal M, White PJ, Tremblay C, St-Amour I, Chevrier G, Emond V, Lefrançois D, et al. (2014) Insulin reverses the high-fat diet-induced increase in brain aβ and improves memory in an animal model of Alzheimer disease. Diabetes 63, 4291–301. [PubMed: 25008180]

Vossel KA, Beagle AJ, Rabinovici GD, Shu H, Lee SE, Naasan G, Hegde M, et al. (2013) Seizures and epileptiform activity in the early stages of Alzheimer disease. JAMA Neurol 70, 1158–66. [PubMed: 23835471]

Yang T, Li S, Xu H, Walsh DM, Selkoe DJ (2017) Large Soluble Oligomers of Amyloid β-Protein from Alzheimer Brain Are Far Less Neuroactive Than the Smaller Oligomers to Which They Dissociate. J. Neurosci 37, 152–163. [PubMed: 28053038]

Zhang S, Chai R, Yang Y-Y, Guo S-Q, Wang S, Guo T, Xu S-F, Zhang Y-H, Wang Z-Y, Guo C (2017) Chronic diabetic states worsen Alzheimer neuropathology and cognitive deficits accompanying disruption of calcium signaling in leptin-deficient APP/PS1 mice. Oncotarget 8, 43617–43634. [PubMed: 28467789]

Zhao W-Q, Townsend M (2009) Insulin resistance and amyloidogenesis as common molecular foundation for type 2 diabetes and Alzheimer's disease. Biochim. Biophys. Acta 1792, 482–96. [PubMed: 19026743]

Zhou Y, Danbolt NC (2013) GABA and Glutamate Transporters in Brain. Front. Endocrinol. (Lausanne) 4, 165. [PubMed: 24273530]

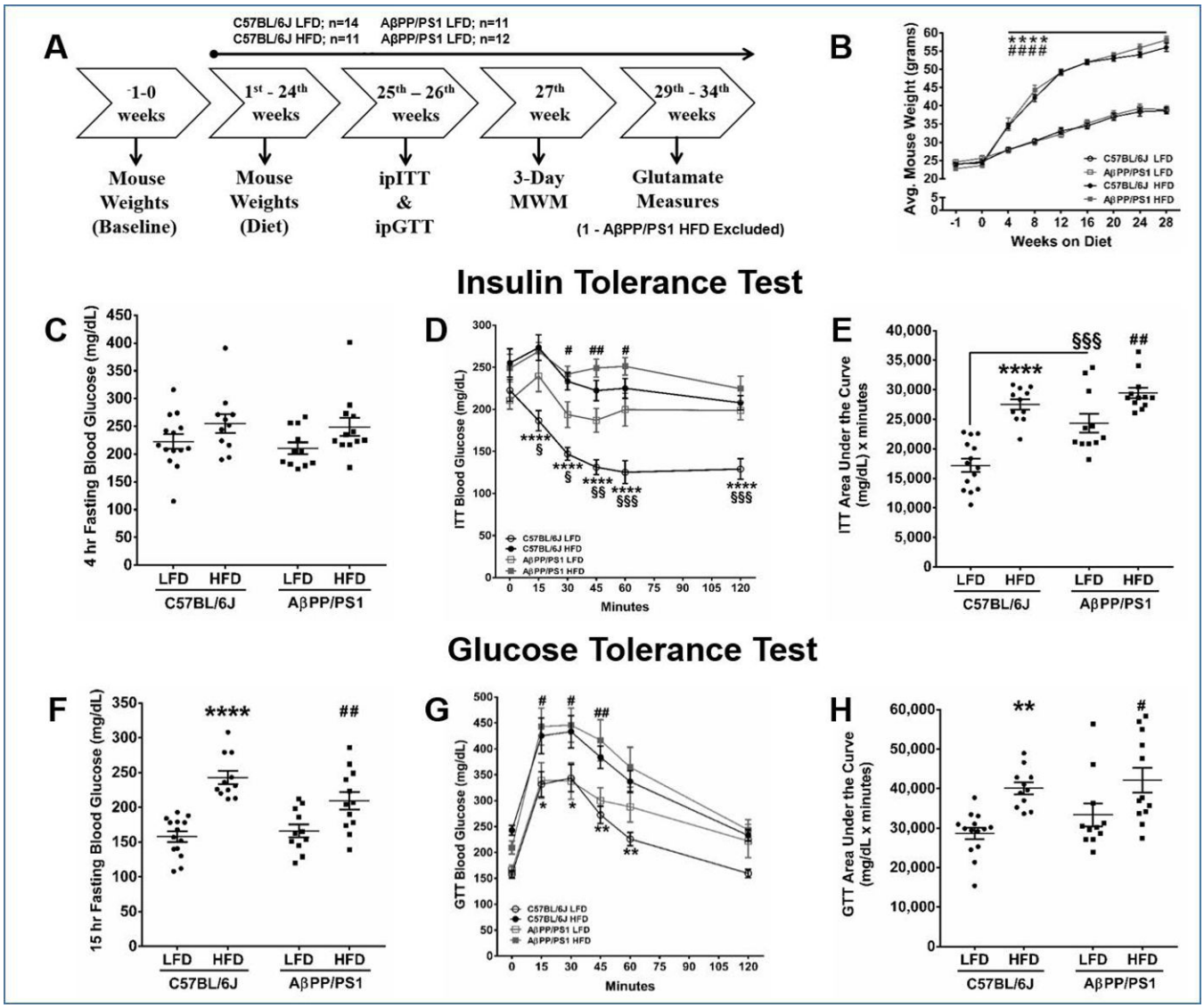

Figure 1: Experimental Design, Mouse Weight, and Blood Glucose Measurements

A) An outline of the experimental design. Abbreviations: intraperitoneal insulin tolerance test (ipITT), intraperitoneal glucose tolerance test (ipGTT), Morris water maze (MWM). B) Analysis of mouse weight gain through 28 weeks on either LFD or HFD. Results from the four hour fasting ipITT and 15 hour fasting ipGTT. Mouse genotypes and diet group are indicated on each graph. C) Four hour fasting blood glucose prior to ip injection of 1 IU/kg b.w. of insulin, D) blood glucose during the 120 minute ipITT, E) area under the curve of the 120 minute ipITT, F) Fifteen hour fasting blood glucose prior to ip injection of 2 g/kg b.w. of glucose, G) blood glucose during the 120 minute ipGTT, H) area under the curve of the 120 minute ipGTT. *p<0.05, **p<0.01, ****p<0.0001 C57BL/6J LFD (n=14) vs C57BL/6J HFD (n=11); #p<0.05, ##p<0.01, ####p<0.0001 AβPP/PS1 LFD (n=11) vs AβPP/PS1 HFD (n=12); §p<0.05, §§p<0.01, §§§p<0.001 C57BL/6J LFD vs AβPP/PS1 LFD; where n refers to the number of animals.

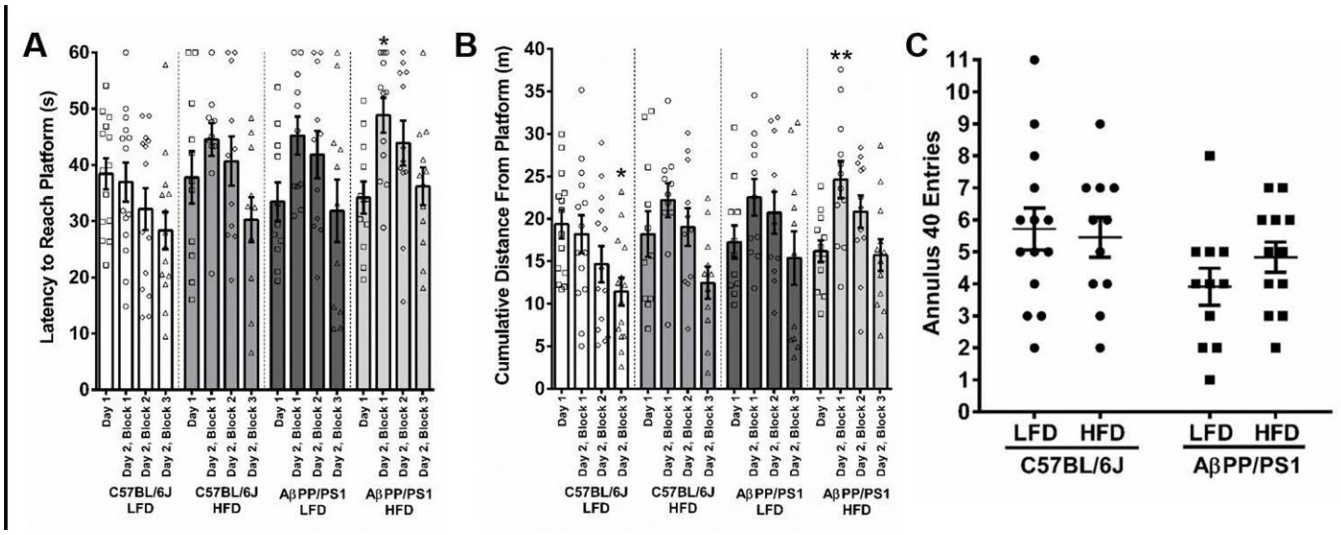

Figure 2: MWM Training and Probe Challenge

The 2-day MWM training session consisted of a visible platform on Day 1 that was changed to a hidden platform on Day 2 and the probe challenge. A) Latency to reach the escape platform for each training session. B) The cumulative distance each mouse spent away from the platform for the training sessions. A & B) *p<0.05, **p<0.01, hidden platform vs Day 1 visible platform. C) The number of annulus 40 crossings. C57BL/6J LFD, n=14; C57BL/6J HFD, n=11; AβPP/PS1 LFD, n=11; AβPP/PS1 HFD, n=12; where n refers to the number of animals.

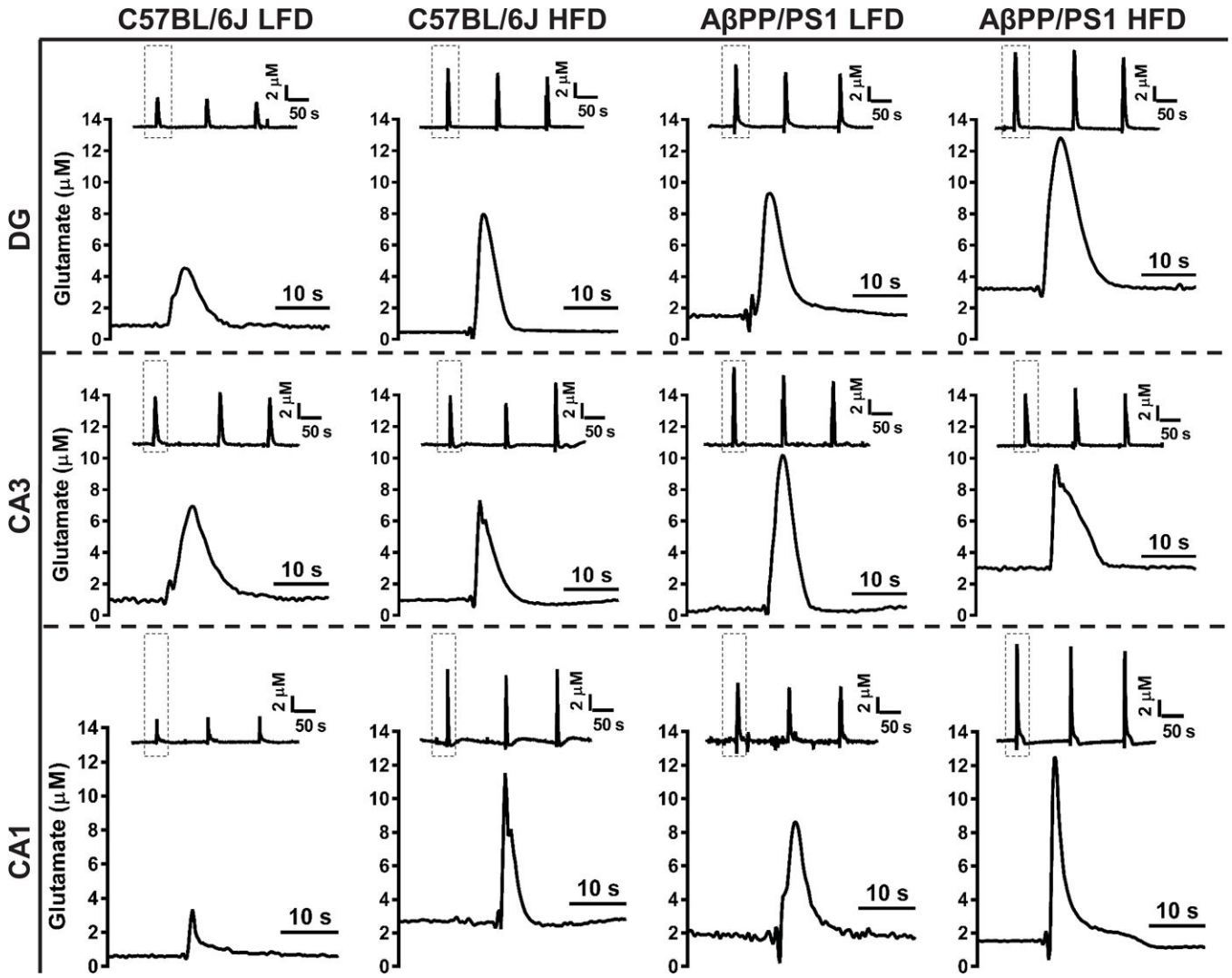

Figure 3: Stimulus-Evoked Glutamate Release Traces

Representative traces of glutamate release from 70 mM KCl stimulation. Columns indicate genotype and diet while rows indicate hippocampal subfield. Within each panel, the inset trace depicts the reproducibility of the glutamate signals with the dashed box indicating a single response magnified beneath for a clearer presentation of glutamate dynamics. Concentration and time axes are consistent in all panels for comparative interpretation.

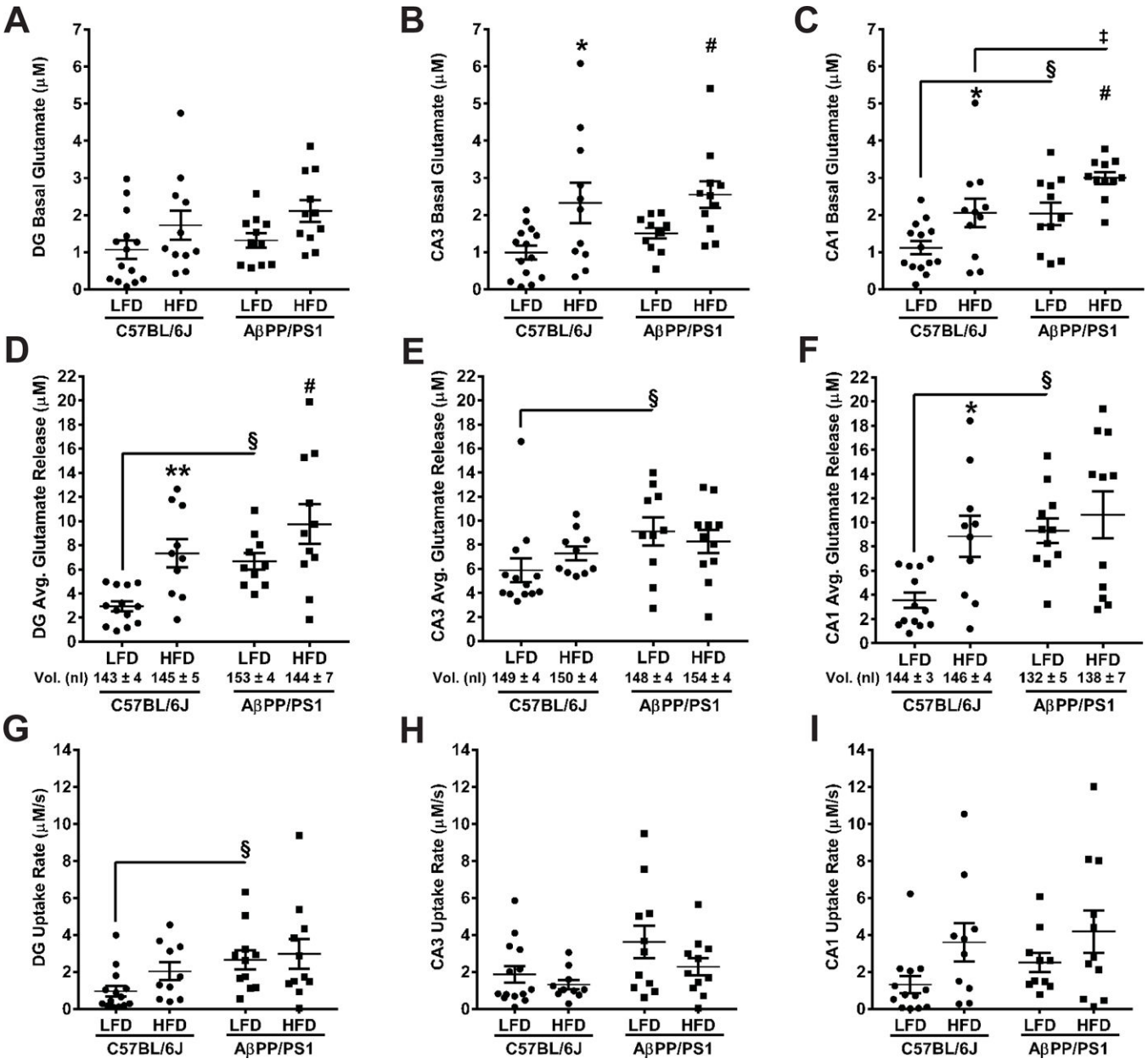

Figure 4: Hippocampal Glutamate Measures

Basal glutamate, stimulus-evoked glutamate release, and evoked glutamate uptake rate in the DG (A, D, G), CA3 (B, E, H), and CA1 (C, F, I). Basal glutamate was measured prior to local application of stimulus. Stimulus volumes (mean ± SEM) are shown beneath the bar graphs in D-F. *p<0.05, **p<0.01 C57BL/6J LFD (n=13–14; 1 subject excluded) vs C57BL/6J HFD (n=10–11; 1 subject excluded); #p<0.05 AβPP/PS1 LFD (n=10–11; 1 subject excluded) vs AβPP/PS1 HFD (n=11; 1 subject died); §p<0.05 C57BL/6J LFD (n=13–14) vs AβPP/PS1 LFD (n=10–11); ‡p<0.05 C57BL/6J HFD (n=10) vs AβPP/PS1 HFD (n=11); where n refers to the number of animals and at most a single subject per group was excluded by Grubb's test.

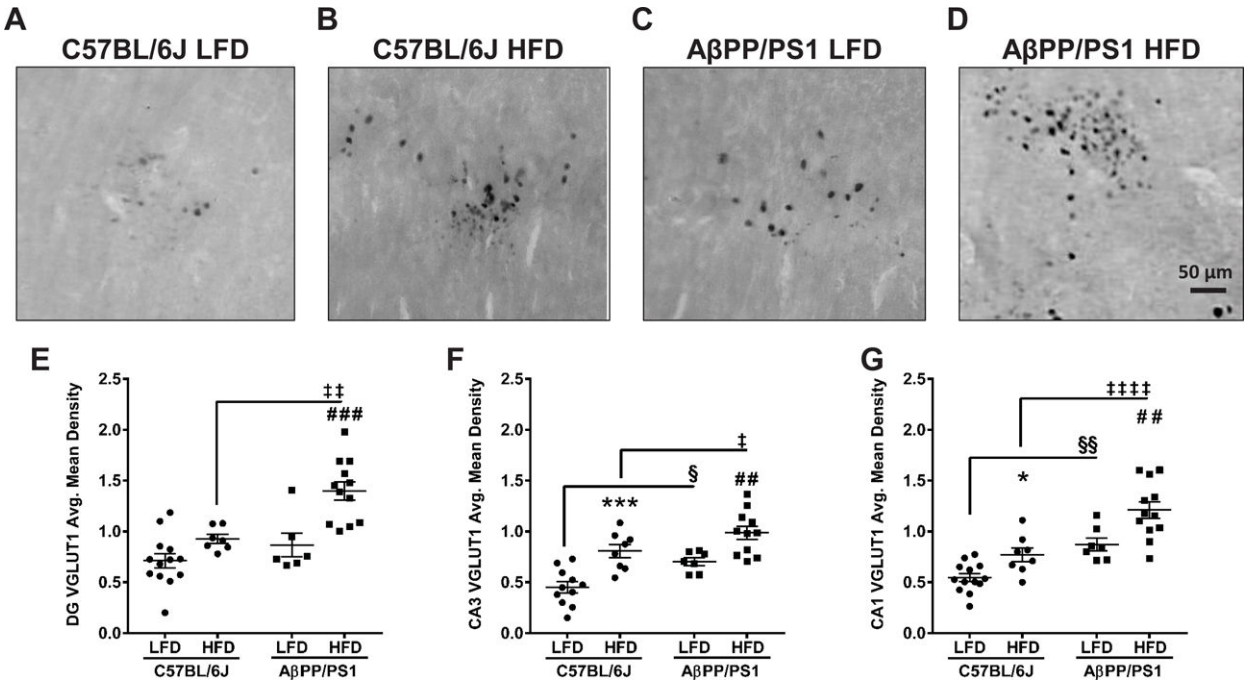

Figure 5: VGLUT1 Immunohistochemistry

Representative images of VGLUT1 staining in the DG at 40x magnification from C57BL/6J LFD (A), C57BL/6J HFD (B), AβPP/PS1 LFD (C), and AβPP/PS1 HFD (D) mice. Scale bar = 50 µm. Average mean density of VGLUT1 staining in the DG (E), CA3 (F), and CA1 (G). *p<0.05, ***p<0.001 C57BL/6J LFD (n=11–13; 1–3 subjects excluded) vs C57BL/6J HFD (n=7–8; 3–4 subjects excluded); ##p<0.01, ###p<0.001 AβPP/PS1 LFD (n=6–7; 4–5 subjects excluded) vs AβPP/PS1 HFD (n=11–12; 1 subject excluded); §p<0.05, §§p<0.01 AβPP/PS1 LFD (n=6–7) vs C57BL/6J LFD (n=11–13); ‡p<0.05, ‡‡p<0.01, ‡‡‡‡p<0.0001 AβPP/PS1 HFD (n=11–12) vs C57BL/6J HFD (n=7–8); where n refers to the number of animals.

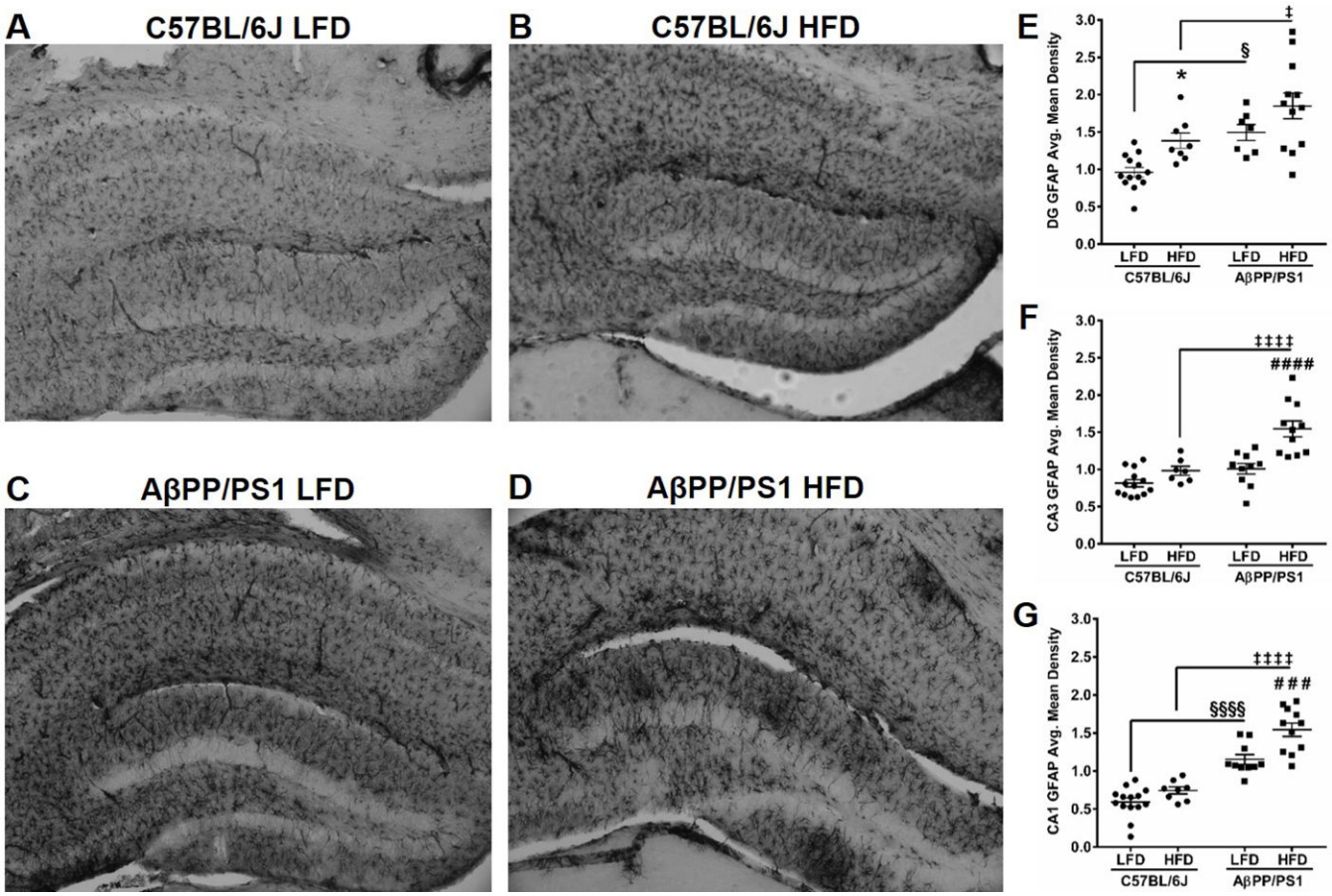

Figure 6: GFAP Immunohistochemistry

Whole hippocampal representative images of GFAP staining in C57BL/6J LFD (A), C57BL/6J HFD (B), AβPP/PS1 LFD (C), and AβPP/PS1 HFD (D) mice at 10x magnification. Average mean density of GFAP staining in the DG (E), CA3 (F), and CA1 (G). *p<0.05 C57BL/6J LFD (n=13–14; 1 subject excluded) vs C57BL/6J HFD (n=7–8; 3–4 subjects excluded); ###p<0.001, ###p<0.0001 AβPP/PS1 LFD (n=7–10, 1–4 subjects excluded) vs AβPP/PS1 HFD (n=11–12; 1 subject excluded); §p<0.05, §§§§p<0.0001 AβPP/PS1 LFD (n=7–10) vs C57BL/6J LFD (n=13–14); ‡p<0.05, ‡‡‡‡p<0.0001 AβPP/PS1 HFD (n=11–12) vs C57BL/6J HFD (n=7–8); where n refers to the number of animals.

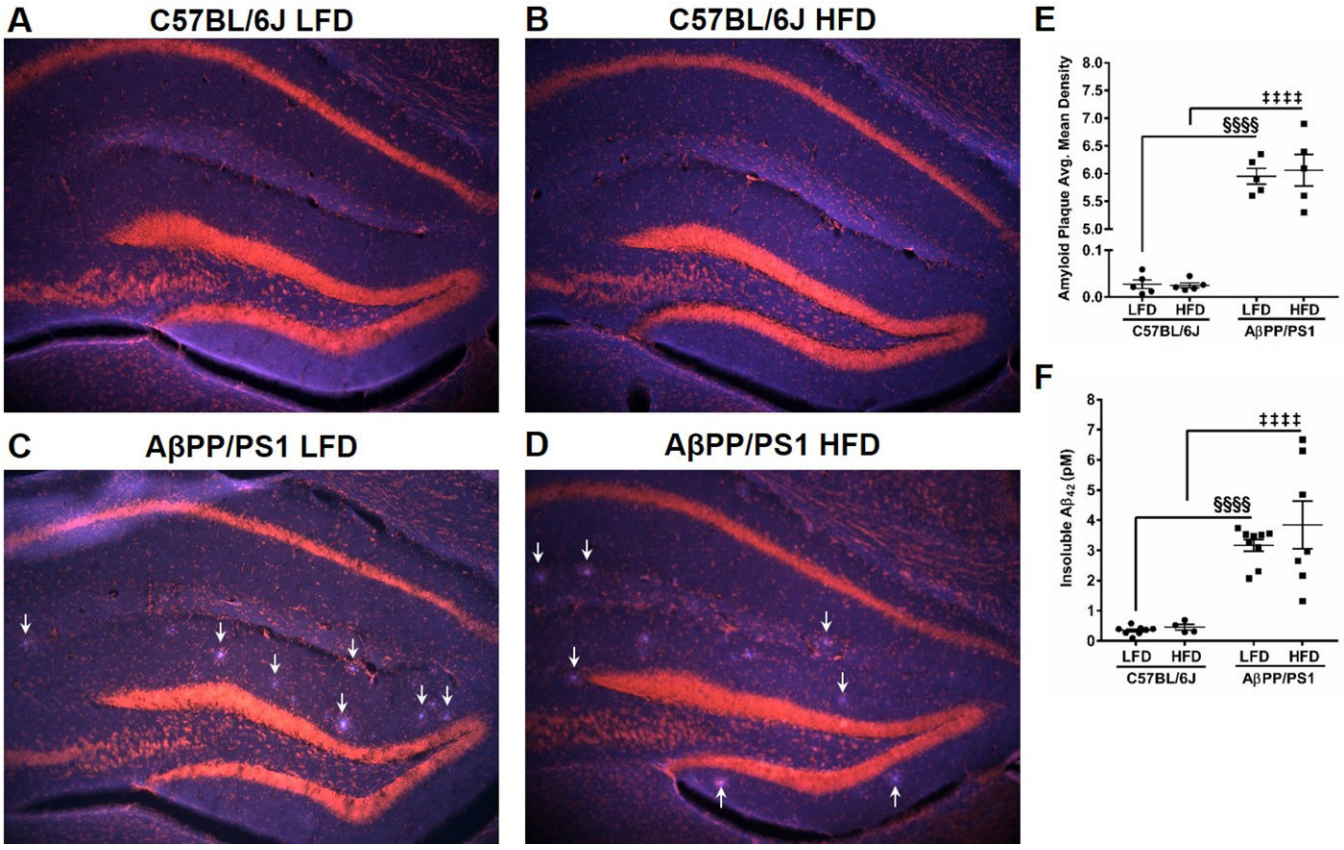

Figure 7: Amyloid Plaque Formation

Whole hippocampal representative images of amyloid plaque formation (blue) and nuclei staining (red) by EtBr in C57BL/6J LFD (A), C57BL/6J HFD (B), AβPP/PS1 LFD (C), and AβPP/PS1 HFD (D) mice at 10x magnification. Arrows indicate plaque formations in C and D. Average mean density of plaque formation in the hippocampus (E) and insoluble $A\beta_{42}$ ELISA determination (F). §§§§p<0.0001 AβPP/PS1 LFD (n=5,9) vs C57BL/6J LFD (n=5,8); ‡‡‡‡p<0.0001 AβPP/PS1 HFD (n=5,7) vs C57BL/6J HFD (n=5,4); where n refers to the number of animals and 7 subjects per group were excluded from IHC plaque analysis.